

## ARTICLE

# Fe<sub>3</sub>O<sub>4</sub>@C@PrNHSO<sub>3</sub>H: A novel magnetically recoverable heterogeneous catalyst in green synthesis of diverse triazoles

Niloufar Nasehi | Behrooz Mirza | Somayeh Soleimani-Amiri

Department of Chemistry, Karaj Branch,  
Islamic Azad University, Karaj, Iran**Correspondence**Behrooz Mirza, Department of Chemistry,  
Karaj Branch, Islamic Azad University,  
Karaj, Iran.  
Email: b.mirza@kiau.ac.ir,  
b\_mirza@azad.ac.ir**Abstract**

The core-shell magnetic nano-catalyst of Fe<sub>3</sub>O<sub>4</sub>@C@PrNHSO<sub>3</sub>H was proposed, synthesized, and fully described by transmission electron microscopy, field-emission scanning electron microscope, energy-dispersive X-ray, vibrating sample magnetometer, thermal gravimetric analysis, X-ray diffraction, Fourier transform infrared, and X-ray photoelectron spectroscopy analysis. Nontoxic texture, magnetic recovery capability, high thermal stability as well as low-cost synthesis method were found as the unique features of the synthesized core-shell magnetic nano-catalyst. Fe<sub>3</sub>O<sub>4</sub>@C@PrNHSO<sub>3</sub>H NPs were introduced as a modern magnetic heterogeneous catalyst in the solvent-free synthesis of triazole derivatives through one-pot, three-component condensation of aldehyde, ammonium acetate, and nicotinic hydrazide. The pleasant yield of products, straightforward work-up, mild reaction conditions, along with magnetically recoverable catalyst were enumerated as the most important advantages of the method. The Fe<sub>3</sub>O<sub>4</sub>@C@PrNHSO<sub>3</sub>H could be easily separated from the reaction mixture by an external magnet and reused six times with the desired catalytic activity.

**KEYWORDS**

core-shell nano-catalyst, green synthesis, heterogeneous catalyst, magnetic nanoparticles, triazoles

## 1 | INTRODUCTION

In recent years, the demand for designing and manufacturing novel catalysts with excellent characteristics such as recyclability, unique molecular architectures, and atom economics to join green chemistry is growing. Heterogeneous catalysts such as metal-organic framework derived catalysts could play a key role in the design of green catalytic protocols due to their recoverability, reusability, and stability in chemical processes.<sup>[1-4]</sup> Those are also widely used in photovoltaic devices, decomposers, sensors, and

batteries.<sup>[5-7]</sup> Heterogeneous catalysts have also been to prominence in the field of heterocyclic synthesis because of mild reaction conditions, cost-effectiveness, simple work-up, atom economy, easy recyclability, and modifiable surface properties.<sup>[8]</sup> Recently, nano-catalysts, with their large surface area and high-density active sites, have emerged as an alternative over various commercial catalysts to develop the catalytic efficiency and application in organic synthesis.<sup>[9-15]</sup> Among numerous species of nano-catalysts, iron oxide nanoparticles (NPs) have achieved much attention due to their idiosyncratic features such as

ease of availability, chemical inertness, high surface area to volume ratio, non-toxicity, excellent thermal stability, magnetic property,<sup>[16]</sup> and also the vast range of applicability in catalysis,<sup>[17–21]</sup> protein separations,<sup>[22]</sup> magnetic resonance imaging (MRI),<sup>[23]</sup> magnetic refrigeration,<sup>[24]</sup> drug delivery,<sup>[25–27]</sup> and magnetic sensors.<sup>[28]</sup> The magnetic nature of iron oxide NPs enables effortless separation from the reaction mixture using an external magnet that not only prevents the cumbersome filtration procedures but also lessens energy consumption, catalyst waste, and saves time in performing catalyst recovery.<sup>[29]</sup> Due to the strong tendency of these magnetic NPs to agglomerate as a result of self-interactions, much effort has been directed toward imparting stability to them via immobilizing the nano-catalysts onto the nano-carriers. To date, many nano-carriers such as surfactant/polymer, silica, metal-organic frameworks, clays, and carbon coating or embedding a matrix/support have been utilized as protection strategies, and the research along this field continues.<sup>[30,31]</sup> It is noteworthy that the protective outer shells produced as a result of coating not only stabilize the NPs but additionally provide active sites for functionalization with other organic groups suitable for desired applications.<sup>[32]</sup> Accordingly, the development of a stable and magnetically retrievable core/shell structured iron oxide nano-catalyst with reusability and recyclability potentials is still challenging, and further, it adds significant value to synthetic organic protocols such as the multicomponent reactions (MCRs).<sup>[33–36]</sup>

In the past decades, MCRs have been considered as one of the most effective and practical routes in organic synthesis from an atom- and step-economical point of view for the construction of heterocycles and natural products such as triazole derivatives.<sup>[37]</sup> It is worthy to mention that among the synthesized heterocyclic compounds, triazole core structures display a diverse array of biological activities in medicinal chemistry, and a large number of triazole-based compounds as clinical drugs such as anticancer, antiviral, anti-inflammatory, antiparasitic, and antimicrobial drugs have been extensively used.<sup>[38–43]</sup> Therefore, developing new approaches for the synthesis of the pharmacologically active triazole derivatives remains to be attractive in contemporary synthetic chemistry. We aim to improve the reaction conditions and scale-up the multicomponent synthesis of triazole building blocks, keeping in view the abovementioned biological activities of them.

Following our studies on the development of magnetic nano-catalysts and their applications in the synthesis of organic compounds,<sup>[44–48]</sup> in this work,  $\text{Fe}_3\text{O}_4@\text{C}@\text{PrNHSO}_3\text{H}$  was synthesized for the first time and applied in the one-pot synthesis of pharmaceutically attractive diverse kinds of triazole derivatives via three-component reactions to investigate the application scope of the novel heterogeneous core-shell magnetic nano-catalyst.

## 2 | RESULT AND DISCUSSIONS

### 2.1 | Synthesis and characterization of $\text{Fe}_3\text{O}_4@\text{C}@\text{PrNHSO}_3\text{H}$

The core-shell magnetic nano-catalyst of  $\text{Fe}_3\text{O}_4@\text{C}@\text{PrNHSO}_3\text{H}$  was synthesized as outlined in Scheme 1. The procedure consists of three steps: (1) Synthesis of core-shell magnetic NPs of  $\text{Fe}_3\text{O}_4@\text{C}$ ; (2) Optimal amination of  $\text{Fe}_3\text{O}_4@\text{C}$  to  $\text{Fe}_3\text{O}_4@\text{C}@\text{PrNH}_2$ ; (3) Optimal sulfonation of  $\text{Fe}_3\text{O}_4@\text{C}@\text{PrNH}_2$  to  $\text{Fe}_3\text{O}_4@\text{C}@\text{PrNHSO}_3\text{H}$ .

The synthesized core-shell magnetic nano-catalyst of  $\text{Fe}_3\text{O}_4@\text{C}@\text{PrNHSO}_3\text{H}$  was characterized by spectral techniques, containing Fourier transform infrared (FT-IR), field-emission scanning electron microscope (FE-SEM), energy-dispersive X-ray (EDX), elemental mapping, vibrating sample magnetometer (VSM), transmission electron microscopy (TEM), thermal gravimetric analysis (TGA), X-ray diffraction (XRD), and X-ray photoelectron spectroscopy (XPS).

#### 2.1.1 | FT-IR analysis

The FT-IR spectra of (a)  $\text{Fe}_3\text{O}_4@\text{C}$ , (b)  $\text{Fe}_3\text{O}_4@\text{C}@\text{PrNH}_2$ , (c)  $\text{Fe}_3\text{O}_4@\text{C}@\text{PrNHSO}_3\text{H}$  NPs, as well as (d) recovered  $\text{Fe}_3\text{O}_4@\text{C}@\text{PrNHSO}_3\text{H}$ , are observed in Figure 1. As illustrated in FT-IR spectrum of  $\text{Fe}_3\text{O}_4@\text{C}$  NPs, a broad band at about  $3,430\text{ cm}^{-1}$  is related to the stretching vibration mode of hydroxyl groups on the surface of NPs (Figure 1a).<sup>[31,44–47]</sup> The bands at  $1,614$ , and  $1,404\text{ cm}^{-1}$  corresponded to  $\text{C}=\text{C}$  stretching vibrations related to carbon shell. The observed signal at  $1,110\text{ cm}^{-1}$  was assigned to the  $\text{C}-\text{O}$  stretching vibrations of  $\text{Fe}_3\text{O}_4@\text{C}$ . The last absorption band at  $\sim 594\text{ cm}^{-1}$  is related to the stretching vibration mode of  $\text{Fe}-\text{O}$  in the core of NPs. Moreover, the appearance of a new absorption band at  $2,924\text{ cm}^{-1}$  in  $\text{Fe}_3\text{O}_4@\text{C}@\text{PrNH}_2$  can be attributed to the  $\text{CH}_2$  stretching vibration (Figure 1b). Also, the strong bands at  $\sim 1,112\text{ cm}^{-1}$  were related to  $\text{SO}_2$  symmetric and asymmetric stretching vibration for both  $\text{Fe}_3\text{O}_4@\text{C}@\text{PrNHSO}_3\text{H}$  and recycled  $\text{Fe}_3\text{O}_4@\text{C}@\text{PrNHSO}_3\text{H}$  (Figure 1c,d).

#### 2.1.2 | EDX analysis and elemental mapping

The EDX spectrum of  $\text{Fe}_3\text{O}_4@\text{C}$  was displayed as Fe (65.1%), O (30.1%), and C (4.8%); while Fe (60.2%), O (30.7%), C (8.2%), Si (0.6%), N (0.4%) were detected for  $\text{Fe}_3\text{O}_4@\text{C}@\text{PrNH}_2$  NPs (Figure 2). The presence of Fe (42.9%), O (24.4%), C (13.6%), Si (12.7%), S (4.3%), and N (2.0%) was clarified for  $\text{Fe}_3\text{O}_4@\text{C}@\text{PrNHSO}_3\text{H}$  NPs by EDX analysis (Figure 2). Moreover, the dispensation

**SCHEME 1** Synthesis procedure of  $\text{Fe}_3\text{O}_4@\text{C}@\text{PrNHSO}_3\text{H}$  NPs

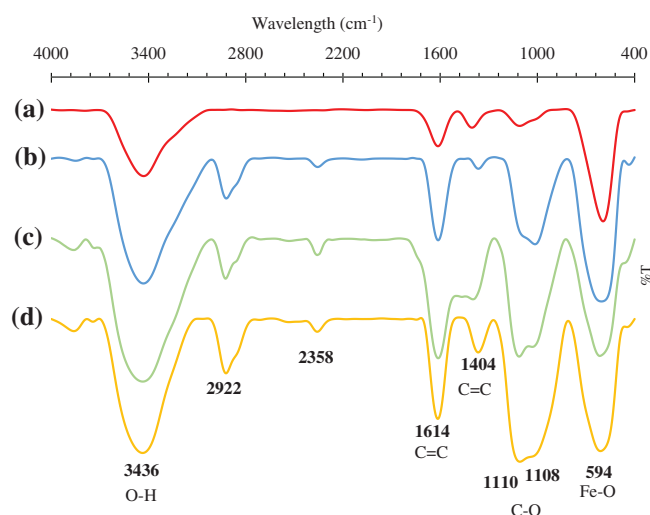
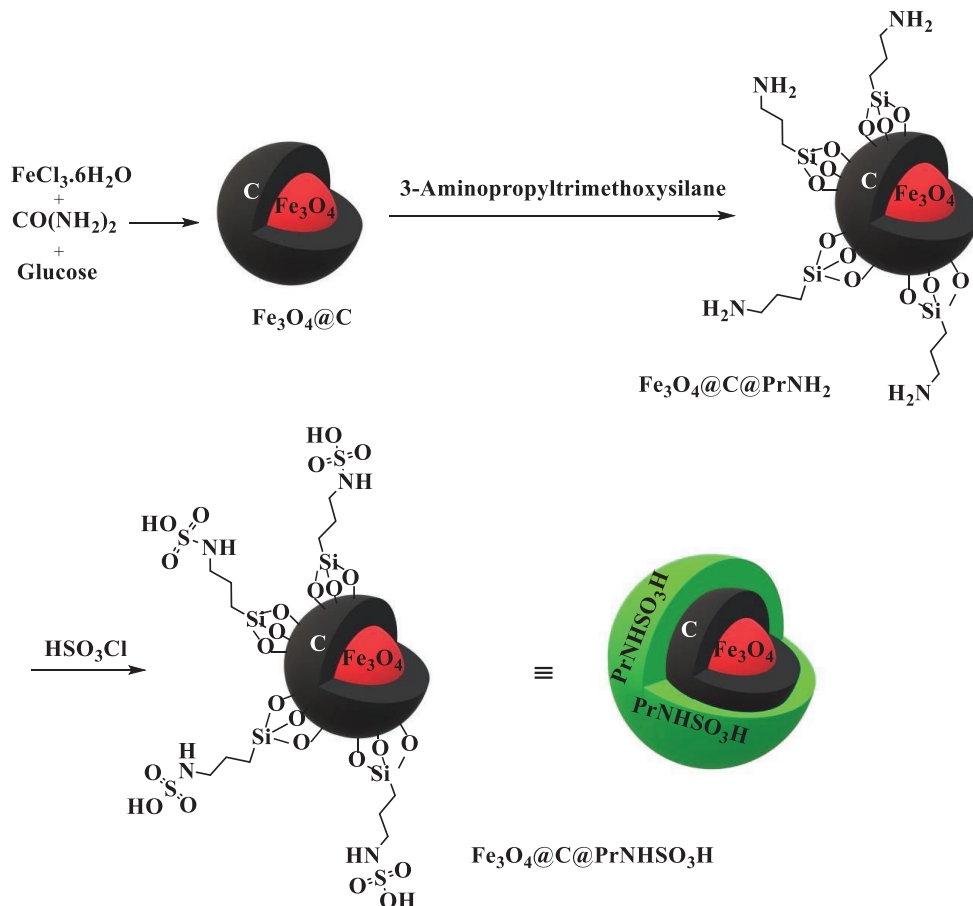


**FIGURE 1** FT-IR spectra of (a)  $\text{Fe}_3\text{O}_4@\text{C}$  NPs; (b)  $\text{Fe}_3\text{O}_4@\text{C}@\text{PrNH}_2$  NPs; (c)  $\text{Fe}_3\text{O}_4@\text{C}@\text{PrNHSO}_3\text{H}$  NPs; and (d) recycled  $\text{Fe}_3\text{O}_4@\text{C}@\text{PrNHSO}_3\text{H}$  NPs after six runs

pattern of the detected structural elements in the  $\text{Fe}_3\text{O}_4@\text{C}@\text{PrNHSO}_3\text{H}$  NPs was well detected via the images of elemental mapping, which confirmed the

uniform distribution of all elements on the surface of  $\text{Fe}_3\text{O}_4@\text{C}@\text{PrNHSO}_3\text{H}$  NPs (Figure 2d).

### 2.1.3 | FE-SEM and TEM images

The morphology evaluation and average particle size of  $\text{Fe}_3\text{O}_4@\text{C}$ ,  $\text{Fe}_3\text{O}_4@\text{C}@\text{PrNH}_2$  and  $\text{Fe}_3\text{O}_4@\text{C}@\text{PrNHSO}_3\text{H}$  NPs were visualized by FE-SEM and TEM images. The FE-SEM images of all three NPs displayed spherical morphology and typical uniformity with a mean size  $\sim 25$ ,  $\sim 41$ , and  $\sim 64$  nm for  $\text{Fe}_3\text{O}_4@\text{C}$ ,  $\text{Fe}_3\text{O}_4@\text{C}@\text{PrNH}_2$ , and  $\text{Fe}_3\text{O}_4@\text{C}@\text{PrNHSO}_3\text{H}$ , respectively (Figure 3). The FE-SEM images also showed some aggregations on the surface of NPs. TEM images of  $\text{Fe}_3\text{O}_4@\text{C}@\text{PrNHSO}_3\text{H}$  NPs are shown in Figure 4. These images verified the spherical core-shell structure of these NPs, so that  $\text{Fe}_3\text{O}_4$  black cores were covered by gray shells.

### 2.1.4 | XRD analysis

A comparison of the XRD analysis of  $\text{Fe}_3\text{O}_4@\text{C}$ ,  $\text{Fe}_3\text{O}_4@\text{C}@\text{PrNH}_2$ ,  $\text{Fe}_3\text{O}_4@\text{C}@\text{PrNHSO}_3\text{H}$ , and recovered

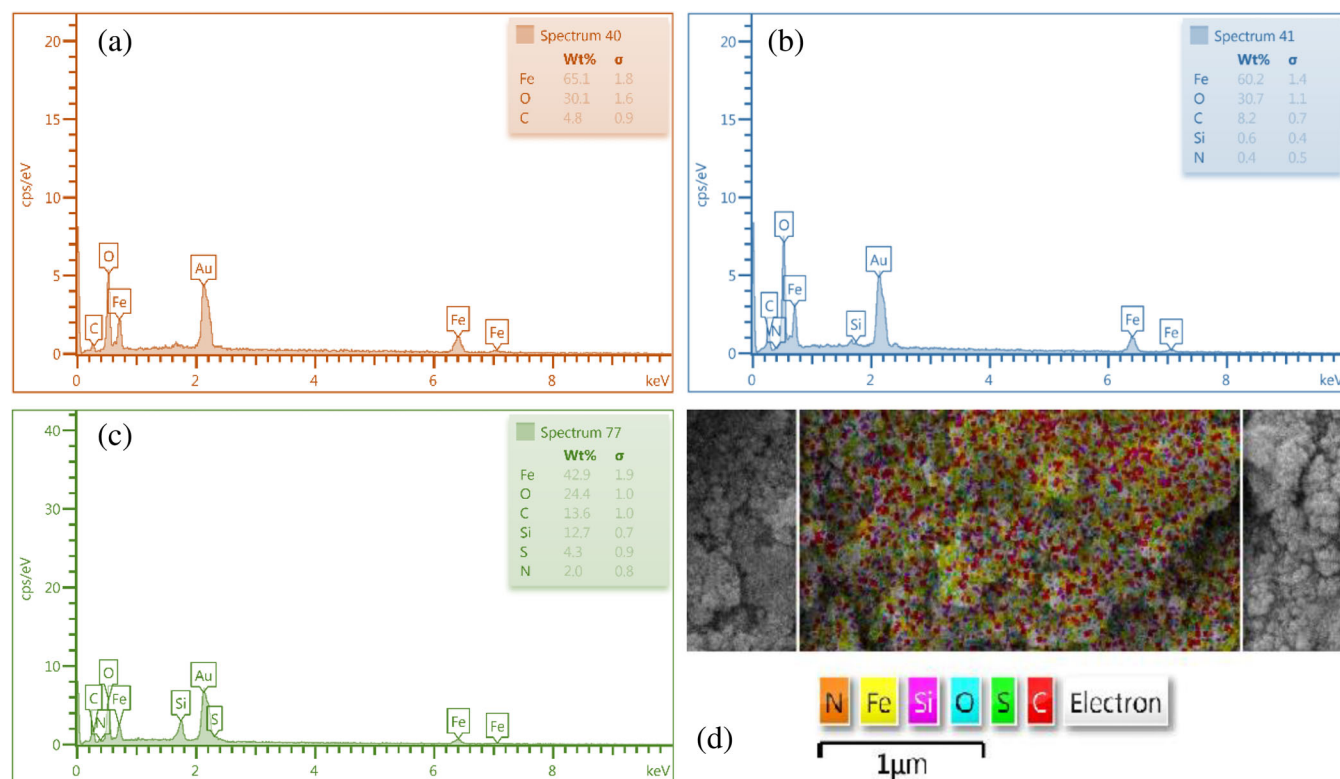


**FIGURE 2** EDX spectra of (a) Fe<sub>3</sub>O<sub>4</sub>@C NPs; (b) Fe<sub>3</sub>O<sub>4</sub>@C@PrNH<sub>2</sub> NPs; and (c) Fe<sub>3</sub>O<sub>4</sub>@C@PrNHSO<sub>3</sub>H NPs; along with (d) elemental mapping of Fe<sub>3</sub>O<sub>4</sub>@C@PrNHSO<sub>3</sub>H NPs

Fe<sub>3</sub>O<sub>4</sub>@C@PrNHSO<sub>3</sub>H is shown in Figure 5. XRD patterns of all the above NPs demonstrated high purity of magnetite without any hematite phase or iron hydroxide phase. Those identified as cubic magnetite crystalline structure of Fe<sub>3</sub>O<sub>4</sub> with six separate diffraction peaks appeared at Bragg angles of  $2\theta$ —30.31°, 35.78°, 43.44°, 53.75°, 57.30°, and 62.97° corresponding to Miller indices of (220), (311), (400), (422), (511), and (440), which was in accordance with Fe<sub>3</sub>O<sub>4</sub> reference code: 01-075-0449. Also, the cubic crystalline structure with a space group of Fd-3m, and space group number of 227 was detected for three types of NPs at:  $a$ : 8.3200 Å,  $b$ : 8.3200 Å,  $c$ : 8.3200 Å,  $\alpha$ : 90.0000°,  $\beta$ : 90.0000°,  $\gamma$ : 90.0000°, with a calculated density of 5.34 g/cm<sup>3</sup>, volume cell of  $575.93 \times 10^6$  p.m.<sup>3</sup>,  $z$ : 8, RIR: 5.03, along with ICSD collection code of 029129. The broad bands in the range of 10°–25° were appointed to amorphous carbon coating on the Fe<sub>3</sub>O<sub>4</sub> NPs.<sup>[31,44–47]</sup> Although, according to the results, the Fe<sub>3</sub>O<sub>4</sub> core structure has been preserved even with surface modifications, in comparison with Fe<sub>3</sub>O<sub>4</sub>@C, there were diminished peak intensity due to the shielding effect of diverse shells. Moreover, there were the same signals for the recycled Fe<sub>3</sub>O<sub>4</sub>@C@PrNHSO<sub>3</sub>H NPs after six runs of the model reaction of triazole synthesis.

Moreover, an estimation of the crystalline size was derived from the Scherrer equation.<sup>[44–46]</sup> Accordingly,

the crystalline size of Fe<sub>3</sub>O<sub>4</sub>@C, Fe<sub>3</sub>O<sub>4</sub>@C@PrNH<sub>2</sub>, and Fe<sub>3</sub>O<sub>4</sub>@C@PrNHSO<sub>3</sub>H was determined about 10.1, 10.8, and 11.3 nm, which detect no significant change in crystal size during modification processes.

### 2.1.5 | VSM analysis

The magnetic features of the produced Fe<sub>3</sub>O<sub>4</sub>@C, Fe<sub>3</sub>O<sub>4</sub>@C@PrNH<sub>2</sub>, Fe<sub>3</sub>O<sub>4</sub>@C@PrNHSO<sub>3</sub>H, and recovered Fe<sub>3</sub>O<sub>4</sub>@C@PrNHSO<sub>3</sub>H were measured by VSM analysis at room temperature and air atmosphere between –15 and 15 kOe (Figure 6). Magnetic hysteresis loops displayed super-paramagnetic behavior for all the mentioned NPs. The saturation magnetization of Fe<sub>3</sub>O<sub>4</sub>@C, Fe<sub>3</sub>O<sub>4</sub>@C@PrNH<sub>2</sub>, Fe<sub>3</sub>O<sub>4</sub>@C@PrNHSO<sub>3</sub>H, and recovered Fe<sub>3</sub>O<sub>4</sub>@C@PrNHSO<sub>3</sub>H was found about 65.77, 55.09, 34.27, and 48.42 emu/g, respectively. The highest magnetic property of 65.77 emu/g was observed for Fe<sub>3</sub>O<sub>4</sub>@C, while it decreased to 55.09 emu/g due to modification with (3-Aminopropyl)trimethoxysilane. Subsequently, the lowest saturation magnetization of 34.27 emu/g was detected for Fe<sub>3</sub>O<sub>4</sub>@C@PrNHSO<sub>3</sub>H owing to a reaction with chlorosulfuric acid. Moreover, 48.42 emu/g magnetization was found for recycled Fe<sub>3</sub>O<sub>4</sub>@C@PrNHSO<sub>3</sub>H, which could be due to the partial

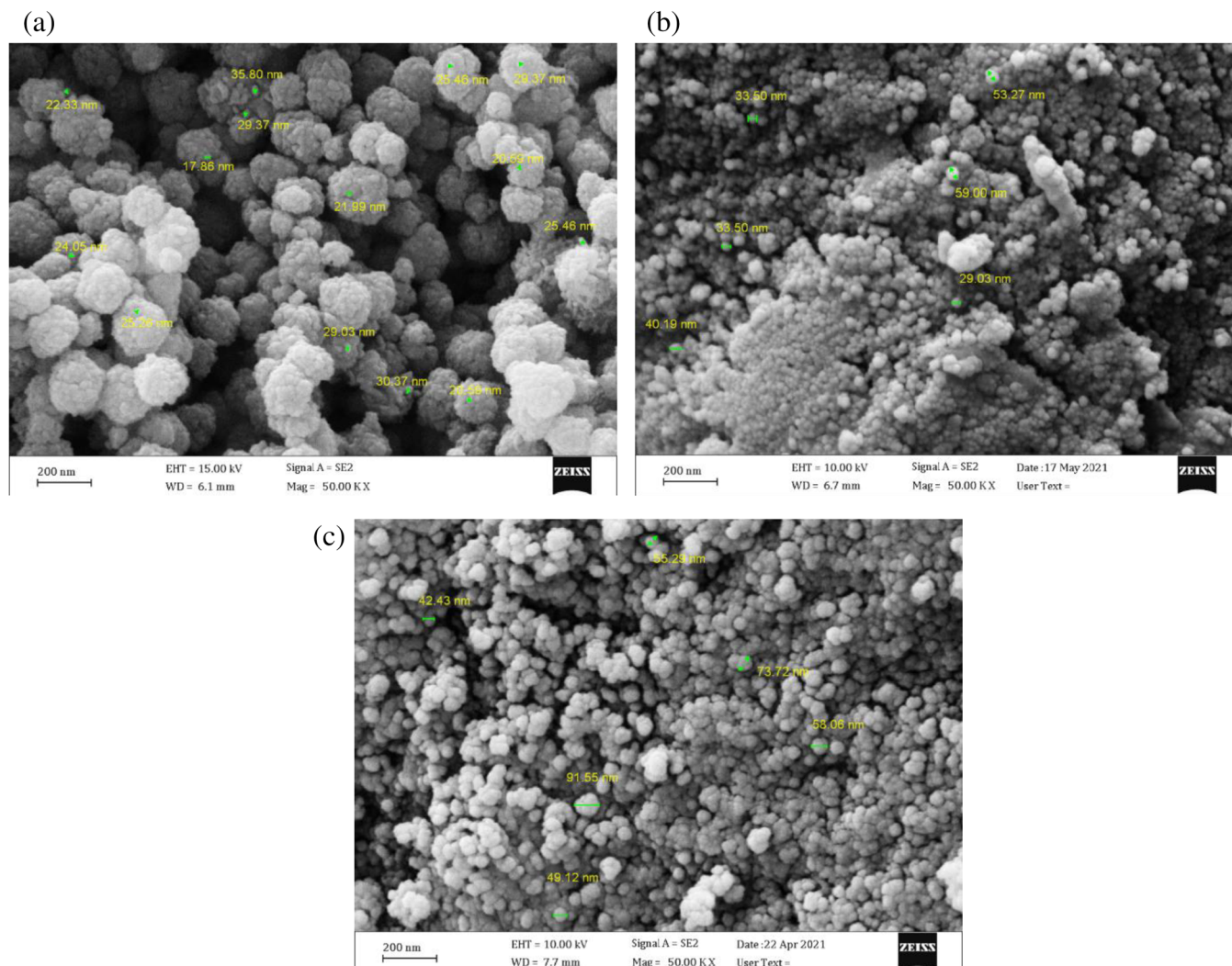


FIGURE 3 FE-SEM images of (a)  $\text{Fe}_3\text{O}_4@C$  NPs; (b)  $\text{Fe}_3\text{O}_4@C@PrNH_2$  NPs; and (c)  $\text{Fe}_3\text{O}_4@C@PrNH_3O_3H$  NPs

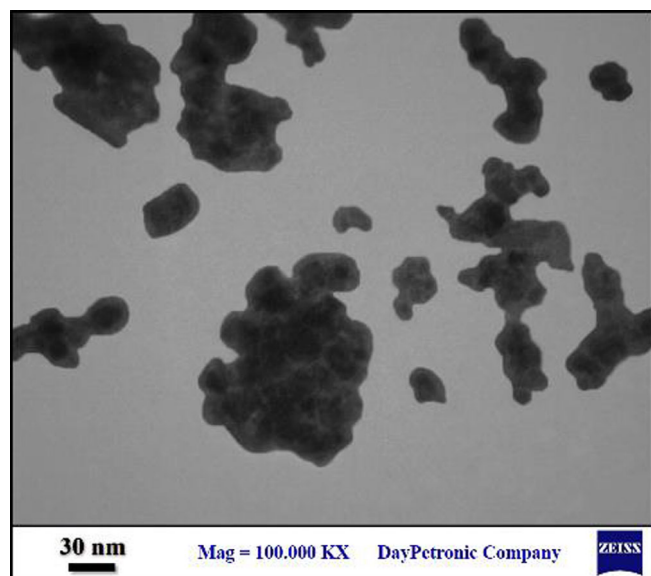


FIGURE 4 TEM images of  $\text{Fe}_3\text{O}_4@C@PrNH_3O_3H$  NPs

separation of the shell from the surface of NPs. Therefore, all four types of applied NPs can be easily removed from the reaction mixture due to their strong magnetization.

### 2.1.6 | TGA and derivative thermal gravimetric

The thermal stability of  $\text{Fe}_3\text{O}_4@C@PrNH_3O_3H$  NPs was investigated by TGA and derivative thermal gravimetric (DTG) analyses in a range of 25–800°C under the air atmosphere (Figure 7). According to the TGA/DTG curves, the first weight loss was observed at 1.94% at around 30–110°C, which was related to the endothermic loss of hydroxyl groups and removal of water molecules in the surface of  $\text{Fe}_3\text{O}_4@C@PrNH_3O_3H$  NPs.<sup>[31,45,46]</sup> The TGA/DTG diagram presented 4.33% weight loss at ~240–490°C, which was attributed to the decomposition of organic groups, sulfonamide, and sulfonic acid groups along with amorphous

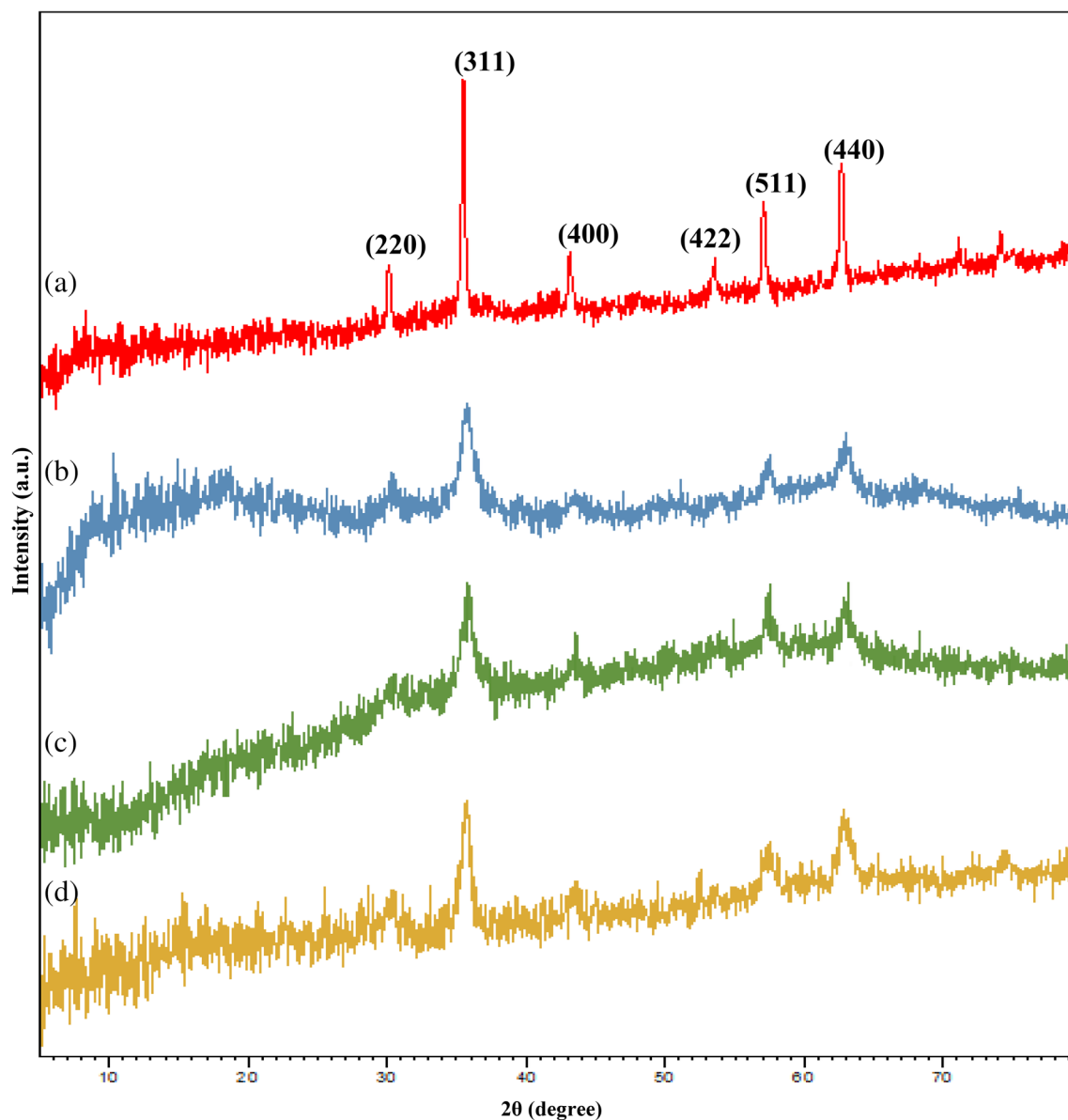


FIGURE 5 XRD patterns of (a)  $\text{Fe}_3\text{O}_4@\text{C}$  NPs; (b)  $\text{Fe}_3\text{O}_4@\text{C}@\text{PrNH}_2$  NPs; (c)  $\text{Fe}_3\text{O}_4@\text{C}@\text{PrNHSO}_3\text{H}$  NPs; and (d) recycled  $\text{Fe}_3\text{O}_4@\text{C}@\text{PrNHSO}_3\text{H}$  after six runs

carbon shells of  $\text{Fe}_3\text{O}_4@\text{C}@\text{PrNHSO}_3\text{H}$  NPs. Therefore, 87.28% residue weight was observed, which indicates the high thermal stability of  $\text{Fe}_3\text{O}_4@\text{C}@\text{PrNHSO}_3\text{H}$  NPs.

### 2.1.7 | X-ray photoelectron spectroscopy

The elemental composition of  $\text{Fe}_3\text{O}_4@\text{C}@\text{PrNHSO}_3\text{H}$  NPs was investigated by the XPS spectrum (Figure 8). The most critical photoelectron peaks of 285, 532, 710, and 725 eV were assigned to C 1s, O 1s, Fe 2p<sub>2/3</sub>, and Fe 2p<sub>1/2</sub>, respectively.<sup>[49,50]</sup> The signals at 711.6 and 726.2 eV could be ascribed to Fe<sup>3+</sup> species, while the peaks at 710.5 and 725.9 eV were attributed to Fe<sup>+2</sup> to

confirm that they correspond to  $\text{Fe}_3\text{O}_4$  core. The XPS of O 1s revealed two peaks at 530.2 and 532.1 eV. Also, two peaks of 282.1 and 285 eV were assigned for C 1s.

## 2.2 | Synthesis of triazole derivatives using $\text{Fe}_3\text{O}_4@\text{C}@\text{PrNHSO}_3\text{H}$

The MCR of benzaldehyde (1), nicotinic hydrazide (2), and ammonium acetate (3) was selected as the model reaction and applied for optimization of the reaction parameters under different conditions (Table 1). The model reaction was examined with different amounts of raw materials, various catalysts, altered catalyst loadings,

**FIGURE 6** VSM analysis of (a)  $\text{Fe}_3\text{O}_4@\text{C}$  NPs; (b)  $\text{Fe}_3\text{O}_4@\text{C}@\text{PrNH}_2$  NPs; (c)  $\text{Fe}_3\text{O}_4@\text{C}@\text{PrNHSO}_3\text{H}$  NPs; and (d) recovered  $\text{Fe}_3\text{O}_4@\text{C}@\text{PrNHSO}_3\text{H}$  NPs after six runs

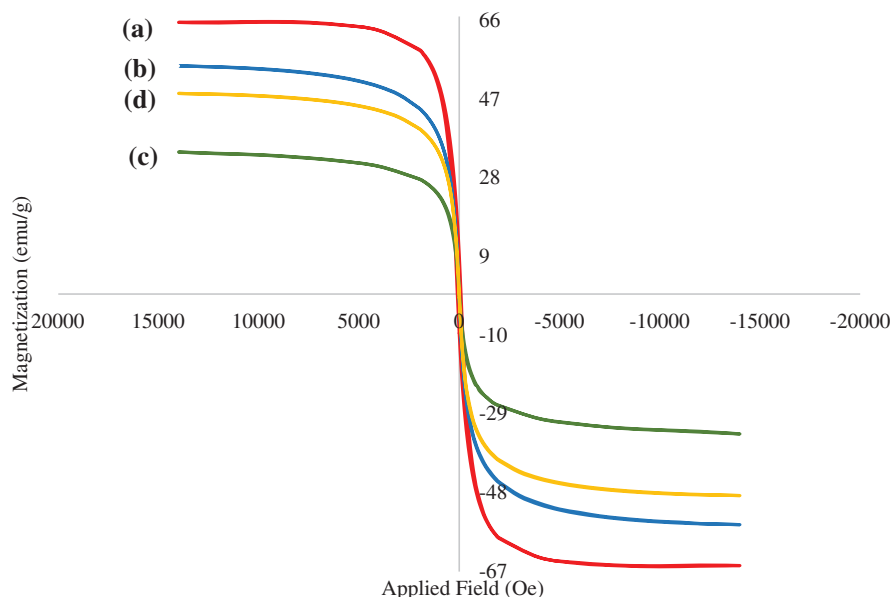
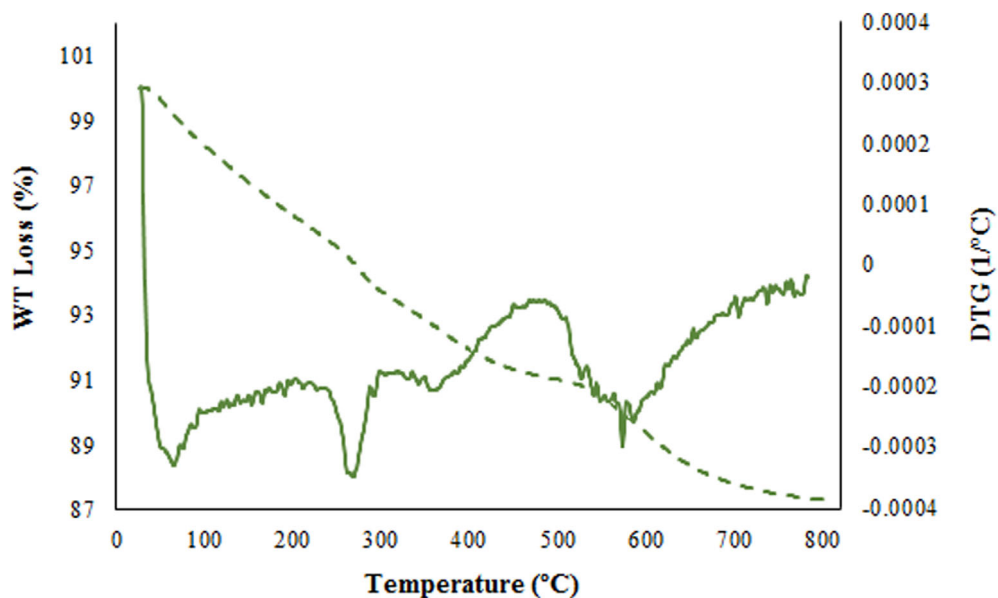


**FIGURE 7** TGA (dashed line) and DTG (solid line) diagrams of  $\text{Fe}_3\text{O}_4@\text{C}@\text{PrNHSO}_3\text{H}$  NPs



various temperatures, and in the presence of different solvents as well as solvent-free conditions in order to improve the reaction conditions. First, the model reaction was carried out in the presence of  $\text{Fe}_3\text{O}_4@\text{C}@\text{PrNHSO}_3\text{H}$  NPs using  $\text{H}_2\text{O}$ , EtOH, acetonitrile, toluene, and DMSO as solvents under several temperatures (Table 1, entries 1–8). Low yields of products were found in the presence of various solvents, which improved with increasing temperature and the amount of catalyst used. The reaction was performed under solvent-free conditions at  $100^\circ\text{C}$ , using 0.06 g catalyst loading of  $\text{Fe}_3\text{O}_4@\text{C}@\text{PrNHSO}_3\text{H}$  NPs with high efficiency of the product (Table 1, entry 9). The reaction efficiency decreased following a reduction in the catalyst consumption or the absence of the catalyst (Table 1, entries 10–11). The condensation of benzaldehyde (**1**; 1 mmol),

nicotinic hydrazide (**2**; 1 mmol), and ammonium acetate (**3**; 2.5 mmol) using  $\text{Fe}_3\text{O}_4@\text{C}@\text{PrNHSO}_3\text{H}$  NPs (0.06 g) at  $100^\circ\text{C}$  under solvent-free conditions with 95% yield of product was introduced as the optimized conditions (Table 1, entry 12).

Next,  $\text{Fe}_3\text{O}_4@\text{C}@\text{PrNHSO}_3\text{H}$  NPs were compared with the other catalysts used in previous articles for synthesis of 3-(3-phenyl-1H-1,2,4-triazol-5-yl)pyridine derivatives (Table 2).<sup>[51,52]</sup> The significant supremacy of  $\text{Fe}_3\text{O}_4@\text{C}@\text{PrNHSO}_3\text{H}$  NPs was detected through the results. Also,  $\text{Fe}_3\text{O}_4@\text{C}@\text{PrNHSO}_3\text{H}$  NPs were evaluated as an efficient catalyst due to magnetic properties followed by convenient separation, production of the high yields of product at a noticeable short reaction time. Also, 3-(3-phenyl-1H-1,2,4-triazol-5-yl)

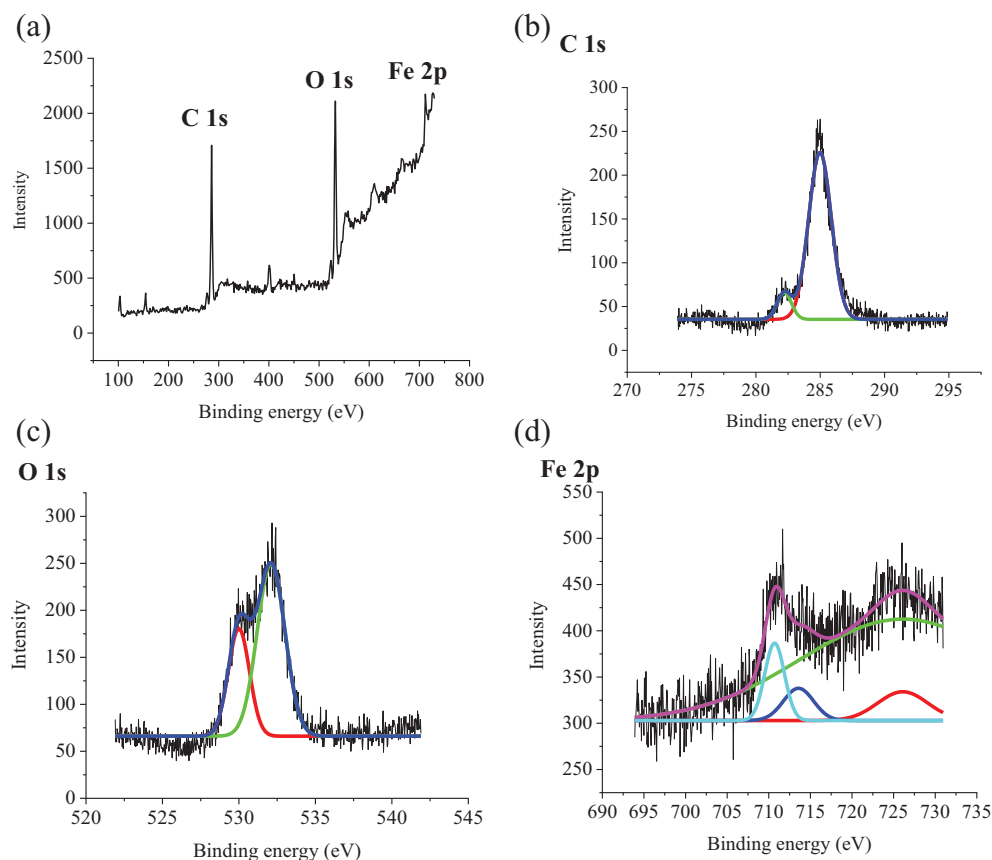


**FIGURE 8** XPS spectra of Fe<sub>3</sub>O<sub>4</sub>@C@PrNHSO<sub>3</sub>H NPs: (a) wide scan XPS spectra; (b) C 1s; (c) O 1s; and (d) Fe 2P spectra

**TABLE 1** The effect of different amounts of raw materials, solvents, temperatures, and catalyst loading in one-pot synthesis of triazole

(1) + (2) + (3) → (4)

Entry	1 (mmol)	2 (mmol)	3 (mmol)	Solvent	T (°C)	Time (min)	Catalyst	Catalyst (g)	Yield (%)
1	1	1	2	Water	R.T.	30	Fe <sub>3</sub> O <sub>4</sub> @C@PrNHSO <sub>3</sub> H	0.03	15
2	1	1	2	Water	60	30	Fe <sub>3</sub> O <sub>4</sub> @C@PrNHSO <sub>3</sub> H	0.03	25
3	1	1	2	Water	100	60	Fe <sub>3</sub> O <sub>4</sub> @C@PrNHSO <sub>3</sub> H	0.03	35
4	1	1	2	Ethanol	100	60	Fe <sub>3</sub> O <sub>4</sub> @C@PrNHSO <sub>3</sub> H	0.06	45
5	1	1	2	Water 1:1 Ethanol	100	60	Fe <sub>3</sub> O <sub>4</sub> @C@PrNHSO <sub>3</sub> H	0.06	50
6	1	1	2	Acetonitrile	100	60	Fe <sub>3</sub> O <sub>4</sub> @C@PrNHSO <sub>3</sub> H	0.06	45
7	1	1	2	Toluene	100	60	Fe <sub>3</sub> O <sub>4</sub> @C@PrNHSO <sub>3</sub> H	0.06	55
8	1	1	2	DMSO	100	60	Fe <sub>3</sub> O <sub>4</sub> @C@PrNHSO <sub>3</sub> H	0.06	60
9	1	1	2	-	100	60	Fe <sub>3</sub> O <sub>4</sub> @C@PrNHSO <sub>3</sub> H	0.06	90
10	1	1	2	-	100	60	Fe <sub>3</sub> O <sub>4</sub> @C@PrNHSO <sub>3</sub> H	0.03	80
11	1	1	2	-	100	60	-	-	43
12	1	1	2.5	-	100	60	Fe <sub>3</sub> O <sub>4</sub> @C@PrNHSO <sub>3</sub> H	0.06	95

**TABLE 2** Screening of some different catalysts in one-pot synthesis of 3-(3-phenyl-1H-1,2,4-triazol-5-yl)pyridine derivatives

Entry	Catalyst	T (°C)	Time (min)	Yield (%)
1	Acetic acid <sup>[51]</sup>	R.T.	24–28 hr	68
2	Glacial acetic acid <sup>[52]</sup>	R.T.	4–6 hr	90
<b>3</b>	<b>Fe<sub>3</sub>O<sub>4</sub>@C@PrNH<sub>3</sub>SO<sub>3</sub>H</b>	<b>100</b>	<b>60</b>	<b>95</b>
4	Fe <sub>3</sub> O <sub>4</sub> @C	100	60	60
5	Fe <sub>3</sub> O <sub>4</sub> @C@PrNH <sub>2</sub>	100	60	64

Note: The bold shows the optimized conditions that was used in the manuscript.

pyridine derivatives were synthesized using Fe<sub>3</sub>O<sub>4</sub>@C@PrNH<sub>3</sub>SO<sub>3</sub>H NPs under solvent-free conditions. As evidenced, the destitute of organic solvents in the reaction has been considered as an important privilege in green chemistry. Moreover, a diminution in reaction efficiency was recognized when Fe<sub>3</sub>O<sub>4</sub>@C and Fe<sub>3</sub>O<sub>4</sub>@C@PrNH<sub>2</sub> NPs were used instead of Fe<sub>3</sub>O<sub>4</sub>@C@PrNH<sub>3</sub>SO<sub>3</sub>H NPs (Table 2, entries 4–5).

The synthesis of diverse triazole derivatives was investigated to expand the scope of the method. Aromatic aldehydes (**1a–1j**; 1 mmol) with varied groups (such as electron-withdrawing and electron-donating and halogen groups), nicotinic hydrazide (**2**; 1 mmol), ammonium acetate (**3**; 2.5 mmol), and Fe<sub>3</sub>O<sub>4</sub>@C@PrNH<sub>3</sub>SO<sub>3</sub>H NPs (0.06 g) were mixed at 100°C to produce different triazole derivatives (**4a–4j**) in 60%–95% yields during 60–90 min (Table 3). Accordingly, some novel products were found in favorable yields and suitable reaction times.<sup>[51–53]</sup>

### 3 | EXPERIMENTAL SECTION

#### 3.1 | Material and equipment

All chemicals and solvents used for the experiment were purchased from Merck and Sigma-Aldrich Companies. The purity of products was observed by thin-layer chromatography (TLC) using silica gel SIL G/UV 254 plates. Melting points were measured using an electro-thermal 9200 apparatus. The Fourier transform infrared (FT-IR) spectra were recorded in the range of 400–4,000 cm<sup>-1</sup> using a PerkinElmer spectrophotometer (Spectrum Two model, United States) by KBr pellets. Nuclear magnetic resonance (<sup>1</sup>H NMR and <sup>13</sup>C NMR) spectra were recorded using Bruker DRX 500 in DMSO solvent. The crystalline structure of the catalyst was examined by X-ray diffraction (XRD) with a Bruker X-ray diffractometer device (D8 Advanced Model, Germany) using Cu-K $\alpha$  radiation ( $\lambda = 0.154$  nm, 40 kV, 30 mA) in the range of

10° ≤ 2 $\theta$  ≤ 80° with 0.5°/s scan rate. A field-emission scanning microscope (FE-SEM) (ZEISS-Sigma VP model, Germany), operating at a 15 kV, was used to visualize the morphology and structure of the nanocrystalline catalysts. The structural elements of each sample were characterized using an energy-dispersive X-ray (EDS) detector (Oxford instrument, England) under standard conditions, attached to the FE-SEM, which is mentioned above. The magnetic properties of the synthesized nano-catalysts were measured using a vibrating sample magnetometer (VSM) of LBKFB model from Meghnatis Daghigh Kavir Company. The thermal gravimetric analysis (TGA) and derivative thermogravimetry (DTG) were found at 15–800°C under air atmosphere using STA1500 model of Rheometric Scientific Co. X-ray photoelectron spectroscopy (XPS) were carried out on an X-ray 8025-BesTec XPS system (Germany) with Mg K $\alpha$  radiation ( $h\nu = 1,253.6$  eV). The binding energy was calibrated internally based on the C 1s line position.

#### 3.2 | Synthesis procedure of Fe<sub>3</sub>O<sub>4</sub>@C@PrNH<sub>3</sub>SO<sub>3</sub>H NPs

The catalyst was prepared in three steps according to Scheme 1. In the first step, the Fe<sub>3</sub>O<sub>4</sub>@C core-shell magnetic NPs were made of iron (III) chloride hexahydrate, glucose, and urea in ethylene glycol solvent by the solvothermal method. In this regard, the FeCl<sub>3</sub>·6H<sub>2</sub>O (1.01 g) was dissolved in ethylene glycol until obtaining an orange color of the mixture, and subsequently, urea (2.25 g) and glucose (0.135 g) were added to the solution under strong stirring. The clear mixture was transferred to an autoclave and heated for 12 hr at 200°C. The black solid product (Fe<sub>3</sub>O<sub>4</sub>@C) was separated by an external magnet and then washed with deionized water and ethanol and dried at 60°C for 6 hr.<sup>[44–47]</sup> In the second step, 0.5 g of the synthesized Fe<sub>3</sub>O<sub>4</sub>@C catalyst was mixed with dry toluene and placed in an ultrasonic bath

TABLE 3 One-pot syntheses of triazole derivatives using  $\text{Fe}_3\text{O}_4@\text{C}@\text{PrNHSO}_3\text{H}$  NPs<sup>a</sup>

Entry	Ar	Product	M.P. (°C) (literature)	Time (min)	Yield <sup>b</sup> (%)
1	$\text{C}_6\text{H}_5$		133–134 (130–132) <sup>[51]</sup>	60	95
	<b>1a</b>	<b>4a</b>			
2	2- $\text{ClC}_6\text{H}_4$		137–140 (138–140) <sup>[51]</sup>	60	60
	<b>1b</b>	<b>4b</b>			
3	3- $\text{ClC}_6\text{H}_4$		>240	60	80
	<b>1c</b>	<b>4c</b>			
4	4- $\text{ClC}_6\text{H}_4$		180–182 (181–183) <sup>[52]</sup>	60	70
	<b>1d</b>	<b>4d</b>			
5	2,4- $\text{Cl}_2\text{C}_6\text{H}_3$		233–235 (232–233) <sup>[53]</sup>	90	90
	<b>1e</b>	<b>4e</b>			
6	3- $\text{BrC}_6\text{H}_4$		205	60	83
	<b>1f</b>	<b>4f</b>			
7	3- $\text{NO}_2\text{C}_6\text{H}_4$		>240	60	95
	<b>1g</b>	<b>4g</b>			
8	3- $\text{OHC}_6\text{H}_4$		188–190	60	60
	<b>1h</b>	<b>4h</b>			

TABLE 3 (Continued)

Entry	Ar	Product	M.P. (°C) (literature)	Time (min)	Yield <sup>b</sup> (%)
9	3-MeC <sub>6</sub> H <sub>4</sub>		140–143	60	74
	<b>1i</b>	<b>4i</b>			
10	C <sub>4</sub> H <sub>3</sub> S		>240	90	79
	<b>1j</b>	<b>4j</b>			

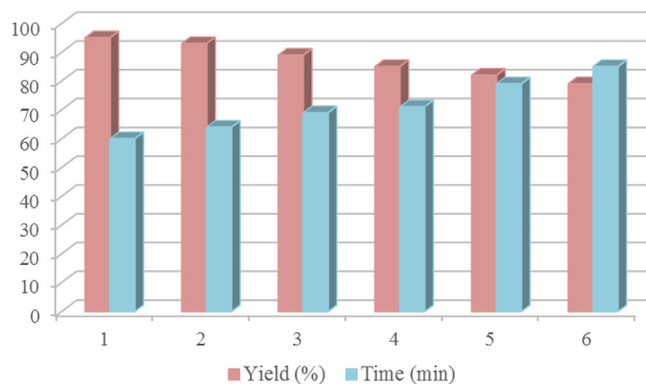
<sup>a</sup>Reaction conditions: Aromatic aldehydes (1 mmol), nicotinic hydrazide (1 mmol), ammonium acetate (2.5 mmol), and Fe<sub>3</sub>O<sub>4</sub>@C@PrNHSO<sub>3</sub>H NPs (0.06 g) at 100°C.

<sup>b</sup>Isolated yields of pure products.

at room temperature for 30 min. Then, 0.5 ml of (3-Aminopropyl)trimethoxysilane (APTMS) was added to it. Subsequently, the resulting solution was refluxed at 100°C for 48 hr. Finally, the resulting precipitate (Fe<sub>3</sub>O<sub>4</sub>@C@PrNH<sub>2</sub>) was removed using a magnet and washed several times with dry toluene, and placed in an oven for hours to dry. In the third step, the resulting Fe<sub>3</sub>O<sub>4</sub>@C@PrNH<sub>2</sub> NPs were added to dichloromethane (45 ml) in a three-neck flask. Then, chloro-sulfonic acid (0.56 ml) was added to the mixture with stirring under atmospheric N<sub>2</sub> gas. After 15 min, when the HCl gas was completely removed, the ultimate NPs (Fe<sub>3</sub>O<sub>4</sub>@C@PrNHSO<sub>3</sub>H NPs) were separated from the mixture utilizing an external magnet. It was washed several times with dichloromethane to remove excess chloro-sulfonic acid and finally dried at room temperature.

### 3.3 | General procedure for the synthesis of triazole derivatives (4a–4j) in the presence of Fe<sub>3</sub>O<sub>4</sub>@C@PrNHSO<sub>3</sub>H NPs

To synthesize the triazole derivatives, aromatic aldehydes (**1a–1j**; 1 mmol), nicotinic hydrazide (**2**; 1 mmol), ammonium acetate (**3**; 2.5 mmol), and Fe<sub>3</sub>O<sub>4</sub>@C@PrNHSO<sub>3</sub>H NPs (0.06 g) were added to the reaction flask under stirring at 100°C. The reaction completion was monitored by TLC. When the reaction was complete (60–90 min), the produced sediments (**4a–4j**) were washed and filtered



SCHEME 2 Reusability of Fe<sub>3</sub>O<sub>4</sub>@C@PrNHSO<sub>3</sub>H NPs during the triazole synthesis

with ethanol/water (1:9) solution. Eventually, the product was dried and purified by a rotary evaporator. All synthesized triazole derivatives were identified by melting points (M.P.), FT-IR, <sup>1</sup>H NMR, and <sup>13</sup>C NMR spectral data.

### 3.4 | Investigation of Fe<sub>3</sub>O<sub>4</sub>@C@PrNHSO<sub>3</sub>H NPs recyclability

The reusability of Fe<sub>3</sub>O<sub>4</sub>@C@PrNHSO<sub>3</sub>H NPs was investigated in the reaction of benzaldehydes (**1a**; 1 mmol), nicotinic hydrazide (**2**; 1 mmol), ammonium acetate (**3**;

2.5 mmol), and  $\text{Fe}_3\text{O}_4@\text{C}@\text{PrNH}_2\text{SO}_3\text{H}$  NPs (0.06 g) at  $100^\circ\text{C}$  as a model reaction (Scheme 2). After reaction completion,  $\text{Fe}_3\text{O}_4@\text{C}@\text{PrNH}_2\text{SO}_3\text{H}$  NPs were removed with an external magnet, washed, and dried to prepare for the next run. The  $\text{Fe}_3\text{O}_4@\text{C}@\text{PrNH}_2\text{SO}_3\text{H}$  NPs could be effectively recycled and reused for six runs without a significant decrease in catalyst activity (Scheme 2).

### 3.5 | The spectral data of some new products

#### 3.5.1 | 3-(3-(3-chlorophenyl)-1H-1,2,4-triazol-5-yl)pyridine (4c)

MP:  $>240^\circ\text{C}$ ; IR (KBr)  $\nu$  ( $\text{cm}^{-1}$ ): 3,787, 3,448, 3,195, 3,016, 1,672, 1,553, 1,418, 1,270, 1,073, 957, 863, 679;  $^1\text{H-NMR}$  (500 MHz,  $\text{DMSO-d}_6$ ,  $\text{Me}_4\text{Si}$ )  $\delta$  (ppm): 7.52 (m, 2H), 7.72 (s, 1H), 7.82–7.84 (m, 2H), 8.46 (s, 1H), 8.79 (m, 2H), 12.22 (bs, 1H);  $^{13}\text{C-NMR}$  (500 MHz,  $\text{DMSO-d}_6$ ,  $\text{Me}_4\text{Si}$ )  $\delta$  (ppm): 122.01, 126.41, 126.96, 130.48, 131.27, 134.16, 136.74, 140.75, 147.77, 150.82, 162.25. MS Calculated for  $\text{C}_{13}\text{H}_9\text{ClN}_4$  ( $[\text{M} + \text{H}]^+$ ) 256.05 found 256. Anal. Calculated for  $\text{C}_{13}\text{H}_9\text{ClN}_4$ : C 60.83; H 3.53; Cl 13.81; N 21.83%. Found: C 61.03; H 3.12; Cl 13.93; N 21.85%.

#### 3.5.2 | 3-(3-(3-bromophenyl)-1H-1,2,4-triazol-5-yl)pyridine (4f)

MP:  $205^\circ\text{C}$  decompose; IR (KBr)  $\nu$  ( $\text{cm}^{-1}$ ): 3,787, 3,464, 3,194, 3,015, 1,674, 1,546, 1,413, 1,264, 1,136, 1,061, 947, 855, 667, 480;  $^1\text{H-NMR}$  (500 MHz,  $\text{DMSO-d}_6$ ,  $\text{Me}_4\text{Si}$ )  $\delta$  (ppm): 7.44–7.96 (m, 5H), 8.44 (s, 1H), 8.80 (m, 2H), 12.21 (bs, 1H);  $^{13}\text{C-NMR}$  (500 MHz,  $\text{DMSO-d}_6$ ,  $\text{Me}_4\text{Si}$ )  $\delta$  (ppm): 122.01, 122.67, 126.83, 129.80, 133.35, 140.74, 147.66, 150.81, 162.25. MS Calculated for  $\text{C}_{13}\text{H}_9\text{BrN}_4$  ( $[\text{M} + \text{H}]^+$ ) 300.00 found 300. Anal. Calculated for  $\text{C}_{13}\text{H}_9\text{BrN}_4$ : C 51.85; H 3.01; Br 26.53; N 18.60%. Found: C 51.78; H 3.11; Br 26.42; N 18.58%.

#### 3.5.3 | 3-(3-(3-nitrophenyl)-1H-1,2,4-triazol-5-yl)pyridine (4g)

MP:  $>240^\circ\text{C}$ ; IR (KBr)  $\nu$  ( $\text{cm}^{-1}$ ): 3,421, 3,235, 3,064, 1,686, 1,529, 1,350, 1,266, 1,141, 1,063, 951, 820, 680;  $^1\text{H-NMR}$  (500 MHz,  $\text{DMSO-d}_6$ ,  $\text{Me}_4\text{Si}$ )  $\delta$  (ppm): 7.42 (m, 2H), 7.84 (m, 2H), 8.01–8.03 (m, 1H), 8.68–8.78 (m, 2H), 8.87 (s, 1H), 12.22 (s, 1H);  $^{13}\text{C-NMR}$  (500 MHz,  $\text{DMSO-d}_6$ ,  $\text{Me}_4\text{Si}$ )  $\delta$  (ppm): 121.97, 127.41, 128.03, 130.36, 131.75, 132.15, 133.87, 140.62, 145.35, 150.00, 150.78, 162.13, 168.43. MS Calculated for  $\text{C}_{13}\text{H}_9\text{N}_5\text{O}_2$  ( $[\text{M} + \text{H}]^+$ ) 267.08 found 267.1.

Anal. Calculated for  $\text{C}_{13}\text{H}_9\text{N}_5\text{O}_2$ : C 58.43; H 3.39; N 26.21; O 11.97%. Found: C 58.12; H 2.98; N 26.45; O 12.07%.

#### 3.5.4 | 3-(5-(pyridin-3-yl)-1H-1,2,4-triazol-3-yl)phenol (4h)

MP:  $188\text{--}190^\circ\text{C}$ ; IR (KBr)  $\nu$  ( $\text{cm}^{-1}$ ): 3,776, 3,428, 3,212, 3,048, 2,928, 2,836, 2,716, 1,651, 1,574, 1,482, 1,407, 1,296, 1,140, 1,057, 967, 789, 681, 481;  $^1\text{H-NMR}$  (500 MHz,  $\text{DMSO-d}_6$ ,  $\text{Me}_4\text{Si}$ )  $\delta$  (ppm): 7.51–7.53 (m, 3H), 7.77–7.82 (m, 3H), 8.45 (s, 1H), 8.77–8.78 (bs, 1H), 12.22 (s, 1H);  $^{13}\text{C-NMR}$  (500 MHz,  $\text{DMSO-d}_6$ ,  $\text{Me}_4\text{Si}$ )  $\delta$  (ppm): 162.11, 150.79, 150.01, 148.12, 140.81, 135.29, 133.42, 131.55, 129.43, 123.51, 121.97. MS Calculated for  $\text{C}_{13}\text{H}_{10}\text{N}_4\text{O}$  ( $[\text{M} + \text{H}]^+$ ) 238.25 found 238. Anal. Calculated for  $\text{C}_{13}\text{H}_{10}\text{N}_4\text{O}$ : C 65.54; H 4.23; N 23.52; O 6.72%. Found: C 65.01; H 3.98; N 23.68; O 7.14%.

#### 3.5.5 | 3-(3-(m-tolyl)-1H-1,2,4-triazol-5-yl)pyridine (4i)

MP:  $140\text{--}143^\circ\text{C}$ ; IR (KBr)  $\nu$  ( $\text{cm}^{-1}$ ): 3,463, 3,197, 3,017, 1,667, 1,558, 1,404, 1,272, 1,063, 773, 680, 443;  $^1\text{H-NMR}$  (500 MHz,  $\text{DMSO-d}_6$ ,  $\text{Me}_4\text{Si}$ )  $\delta$  (ppm): 2.37 (s, 3H), 7.17 (m, 2H), 7.50–7.57 (m, 2H), 8.15 (m, 1H), 8.45–8.70 (m, 2H), 8.35 (s, 1H), 12.27 (bs, 1H);  $^{13}\text{C-NMR}$  (500 MHz,  $\text{DMSO-d}_6$ ,  $\text{Me}_4\text{Si}$ )  $\delta$  (ppm): 162.06, 150.78, 149.55, 140.95, 138.61, 134.46, 131.56, 129.24, 127.97, 125.16, 122.00. MS Calculated for  $\text{C}_{14}\text{H}_{12}\text{N}_4$  ( $[\text{M} + \text{H}]^+$ ) 236.11 found 236. Anal. Calculated for  $\text{C}_{14}\text{H}_{12}\text{N}_4$ : C 71.17; H 5.12; N 23.71%. Found: C 70.97; H 5.45; N 23.86%.

#### 3.5.6 | 3-(3-(thiophen-2-yl)-1H-1,2,4-triazol-5-yl)pyridine (4j)

MP:  $>240^\circ\text{C}$ ; IR (KBr)  $\nu$  ( $\text{cm}^{-1}$ ): 3,936, 3,787, 3,410, 3,236, 2,836, 2,200, 1,687, 1,503, 1,409, 1,266, 1,144, 1,012, 799, 504;  $^1\text{H-NMR}$  (500 MHz,  $\text{DMSO-d}_6$ ,  $\text{Me}_4\text{Si}$ )  $\delta$  (ppm): 7.16 (s, 1H), 7.51–8.78 (m, 6H), 12.01 (bs, 1H);  $^{13}\text{C-NMR}$  (500 MHz,  $\text{DMSO-d}_6$ ,  $\text{Me}_4\text{Si}$ )  $\delta$  (ppm): 121.92, 128.40, 129.90, 132.00, 136.74, 139.20, 140.88, 144.53, 149.85, 150.78, 161.88. MS Calculated for  $\text{C}_{11}\text{H}_8\text{N}_4\text{S}$  ( $[\text{M} + \text{H}]^+$ ) 228.27 found 228. Anal. Calculated for  $\text{C}_{11}\text{H}_8\text{N}_4\text{S}$ : C 57.88; H 3.53; N 24.54; S 14.04%. Found: C 58.05; H 3.72; N 24.37; S 13.84%.

## 4 | CONCLUSIONS

In conclusion,  $\text{Fe}_3\text{O}_4@\text{C}@\text{PrNH}_2\text{SO}_3\text{H}$  was synthesized and introduced as a novel heterogeneous core-shell

magnetic nano-catalyst in the one-pot three-component condensation reaction for the synthesis of triazole derivatives. The beneficial features of the present protocol include separability and reusability of the synthesized nano-catalyst up to the six runs, short reaction time period, excellent product yield, and operational simplicity. Subsequently, the goal to design and prepare a new and effective magnetic nano-catalyst for the green synthesis of triazole derivatives with an increment in yield and reduction in the waste footprint was achieved.

## REFERENCES

- [1] Y.-T. Liao, V. C. Nguyen, N. Ishiguro, A. P. Young, C.-K. Tsung, K. C. W. Wu, *Appl. Catal., B* **2020**, *270*, 118805.
- [2] H. Konnerth, B. M. Matsagar, S. S. Chen, M. H. G. Precht, F.-K. Shieh, K. C. W. Wu, *Coord. Chem. Rev.* **2020**, *416*, 213319.
- [3] L. Song, J. Tang, T. Wang, C. Wu, Y. Ide, J. He, Y. Yamauchi, *Chem. – Eur. J.* **2019**, *25*, 6807.
- [4] E. Doustkhah, J. Lin, S. Rostamnia, C. Len, R. Luque, X. Luo, Y. Bando, K. C.-W. Wu, J. Kim, Y. Yamauchi, Y. Ide, *Chem. – Eur. J.* **2019**, *25*, 1614.
- [5] C.-C. Chueh, C.-I. Chen, Y.-A. Su, H. Konnerth, Y.-J. Gu, C.-W. Kung, K. C. W. Wu, *J. Mater. Chem. A* **2019**, *7*, 17079.
- [6] C.-C. Lee, C.-I. Chen, Y.-T. Liao, K. C.-W. Wu, C.-C. Chueh, *Adv. Sci.* **2019**, *6*, 1801715.
- [7] J. Wang, Y. Xu, B. Ding, Z. Chang, X. Zhang, Y. Yamauchi, K. C.-W. Wu, *Angew. Chem. Int. Ed.* **2018**, *57*, 2894.
- [8] L. Liu, A. Corma, *Chem. Rev.* **2018**, *118*, 4981.
- [9] Z. Li, S. Ji, Y. Liu, X. Cao, S. Tian, Y. Chen, Z. Niu, Y. Li, *Chem. Rev.* **2020**, *120*, 623.
- [10] M. Ghazvini, F. Sheikholeslami-Farahani, S. Soleimani-Amiri, M. Salimifard, R. Rostamian, *Synlett* **2017**, *29*, 493.
- [11] S. Soleimani-Amiri, Z. Hossaini, M. Arabkhazaeli, H. Karami, S. A. S. Abad, *J. Chin. Chem. Soc.* **2019**, *66*, 438.
- [12] S. Soleimani Amiri, *J. Heterocyclic Chem.* **2020**, *57*, 4057.
- [13] S. S. Amiri, M. Ghazvini, S. Khandan, S. Afrashteh, *Polycyclic Aromat. Compd.* **2021**, *1*. <https://doi.org/10.1080/10406638.2021.1912122>
- [14] S. Mohammadi, M. Musavi, F. Abdollahzadeh, S. Babadoust, A. Hosseinian, *Chem. Rev. Lett.* **2018**, *1*, 49.
- [15] S. Ahmadi, A. Hosseinian, P. D. K. Nezhad, A. Monfared, E. Vessally, *Iran. J. Chem. Chem. Eng.* **2019**, *38*, 1.
- [16] Q. Zhang, X. Yang, J. Guan, *ACS Appl. Nano Mater.* **2019**, *2*, 4681.
- [17] V. Polshettiwar, R. Luque, A. Fihri, H. Zhu, M. Bouhrara, J.-M. Basset, *Chem. Rev.* **2011**, *111*, 3036.
- [18] S. Abdolmohammadi, Z. Hossaini, *Mol. Diversity* **2019**, *23*, 885.
- [19] S. Soleimani-Amiri, M. Arabkhazaeli, Z. Hossaini, S. Afrashteh, A. A. Eslami, *J. Heterocyclic Chem.* **2018**, *55*, 209.
- [20] S. Soleimani-Amiri, F. Shafaei, A. Varasteh Moradi, F. Gholami-Orimi, Z. Rostami, *J. Heterocyclic Chem.* **2019**, *56*, 2744.
- [21] W. Ma, A. G. Ebadi, M. S. Sabil, R. Javahershenas, G. Jimenez, *RSC Adv.* **2019**, *9*, 12801.
- [22] S. P. Schwaminger, S. A. Blank-Shim, I. Scheifele, V. Pipich, P. Fraga-García, S. Berensmeier, *Biotechnol. J.* **2019**, *14*, 1800055.
- [23] A. Avasthi, C. Caro, E. Pozo-Torres, M. P. Leal, M. L. García-Martín, *Top. Curr. Chem.* **2020**, *378*, 40.
- [24] T. Prabhakaran, R. V. Mangalaraja, J. C. Denardin, *J. Magn. Magn. Mater.* **2017**, *444*, 297.
- [25] S. Zhao, X. Yu, Y. Qian, W. Chen, J. Shen, *Theranostics* **2020**, *10*, 6278.
- [26] A. A. Hernández-Hernández, G. Aguirre-Álvarez, R. Cariño-Cortés, L. H. Mendoza-Huizar, R. Jiménez-Alvarado, *Chem. Pap.* **2020**, *74*, 3809.
- [27] D. D. Stueber, J. Villanova, I. Aponte, Z. Xiao, V. L. Colvin, *Pharmaceutics* **2021**, *13*, 943.
- [28] T. T. Tung, N. V. Chien, N. Van Duy, N. Van Hieu, M. J. Nine, C. J. Coghlan, D. N. H. Tran, D. Losic, *J. Colloid Interface Sci.* **2019**, *539*, 315.
- [29] R. K. Sharma, S. Dutta, S. Sharma, R. Zboril, R. S. Varma, M. B. Gawande, *Green Chem.* **2016**, *18*, 3184.
- [30] J. Zhang, Q. Fang, J. Duan, H. Xu, H. Xu, S. Xuan, *Langmuir* **2018**, *34*, 4298.
- [31] J. Zheng, Z. Q. Liu, X. S. Zhao, M. Liu, X. Liu, W. Chu, *Nanotechnology* **2012**, *23*, 165601.
- [32] Z. B. Shifrina, V. G. Matveeva, L. M. Bronstein, *Chem. Rev.* **2020**, *120*, 1350.
- [33] S. Fakheri-Vayeghan, S. Abdolmohammadi, R. Kia-Kojoori, *Z. Naturforsch. B* **2018**, *73*, 545.
- [34] F. Chaghari-Farahani, S. Abdolmohammadi, R. Kia-Kojoori, *RSC Adv.* **2020**, *10*, 15614.
- [35] S. Abdolmohammadi, S. Shariati, N. E. Fard, A. Samani, *J. Heterocyclic Chem.* **2020**, *57*, 2729.
- [36] S. Abdolmohammadi, S. Shariati, B. Mirza, *Appl. Organomet. Chem.* **2021**, *35*, e6117.
- [37] Z. Chen, Z. Liu, G. Cao, H. Li, H. Ren, *Adv. Synth. Catal.* **2017**, *359*, 202.
- [38] L.-W. Xia, M.-Y. Ba, W. Liu, W. Cheng, C.-P. Hu, Q. Zhao, Y.-F. Yao, M.-R. Sun, Y.-T. Duan, *Future Med. Chem.* **2019**, *11*, 2919.
- [39] K. Bozorov, J. Zhao, H. A. Aisa, *Bioorg. Med. Chem.* **2019**, *27*, 3511.
- [40] B. Zhang, *Eur. J. Med. Chem.* **2019**, *168*, 357.
- [41] S. Zhang, Z. Xu, C. Gao, Q. C. Ren, L. Chang, Z. S. Lv, L. S. Feng, *Eur. J. Med. Chem.* **2017**, *138*, 501.
- [42] M. Xu, Y. Peng, L. Zhu, S. Wang, J. Ji, K. P. Rakesh, *Eur. J. Med. Chem.* **2019**, *180*, 656.
- [43] M.-T. Fuh, C.-C. Tseng, S.-M. Li, S.-E. Tsai, T.-J. Chuang, C.-H. Lu, Y.-C. Yang, H. J. Tsai, F. F. Wong, *Bioorg. Chem.* **2021**, *114*, 105049.
- [44] H. Ghavidel, B. Mirza, S. Soleimani-Amiri, M. Manafi, *J. Chin. Chem. Soc.* **2020**, *67*, 1856.
- [45] H. Ghavidel, B. Mirza, S. Soleimani-Amiri, *Polycyclic Aromat. Compd.* **2021**, *41*, 604.
- [46] Z. Samiei, S. Soleimani-Amiri, Z. Azizi, *Mol. Diversity* **2021**, *25*, 67.
- [47] S. F. Taheri Hatkehlouei, B. Mirza, S. Soleimani-Amiri, *Polycyclic Aromat. Compd.* **2020**, *1*. <https://doi.org/10.1080/10406638.2020.1781203>.
- [48] P. Kamalzare, B. Mirza, S. Soleimani-Amiri, *J. Nanostruct. Chem.* **2021**, *11*, 229.
- [49] Y. Zhao, H. Zhang, X. Yang, H. Huang, G. Zhao, T. Cong, X. Zuo, Z. Fan, S. Yang, L. Pan, *Carbon* **2021**, *171*, 395.
- [50] M. Periyasamy, S. Sain, U. Sengupta, M. Mandal, S. Mukhopadhyay, A. Kar, *Mater. Adv.* **2021**, *2*, 4843.
- [51] G. Nigade, P. Chavan, M. Deodhar, *Med. Chem. Res.* **2012**, *21*, 27.

[52] S. S. Panda, S. C. Jain, *Med. Chem. Res.* **2014**, 23, 848.

[53] E. Browne, *Aust. J. Chem.* **1975**, 28, 2543.

### SUPPORTING INFORMATION

Additional supporting information may be found in the online version of the article at the publisher's website.

**How to cite this article:** N. Nasehi, B. Mirza, S. Soleimani-Amiri, *J. Chin. Chem. Soc.* **2021**, 1.  
<https://doi.org/10.1002/jccs.202100239>